Prediction of strong solvatochromism in a molecular photocatalyst

Miftahussurur Hamidi Putra,[†] Benedikt Bagemihl,[‡] Sven Rau,[‡] and Axel Groß[*,†,¶]

†Institute of Theoretical Chemistry, Ulm University, 89069 Ulm, Germany

‡Institute of Inorganic Chemistry I, Materials and Catalysis, Ulm University, 89069 Ulm, Germany

¶Helmholtz Institute Ulm (HIU), Electrochemical Energy Storage, 89069 Ulm, Germany

E-mail: Axel.Gross@uni-ulm.de

Abstract

Based on quantum chemical calculations, we predict strong solvatochromism in a light-driven molecular photocatalyst for hydrogen generation, i.e., we show that the electronic and optical properties of the photocatalyst strongly depend on the solvent it is dissolved in. Our calculations in particular indicate a solvent dependent relocation of the highest occupied molecular orbital (HOMO). Ground-state density functional theory and linear response time dependent density functional theory calculations are applied in order to investigate the influence of implicit solvents on the structural, electronic and optical properties of a molecular photocatalyst. Only at high dielectric constants of the solvent, the HOMO is located at the metal center of the photosensitizer, whereas at low dielectric constants the HOMO is centered at the metal atom of the catalytically active complex. We elucidate the electronic origins of this strong solvatochromic effect and sketch the consequences of these insights for the use of photocatalysts in different environments.

Keywords

photocatalysis, solvatochromism, quantum chemistry, implicit solvent, highest occupied molecular orbital

1 Introduction

The efficient direct conversion of sunlight into valuable chemicals is challenging but has the potential to significantly contribute to a carbon-emission free energy economy.[1] Recent years have witnessed an increased understanding of the mechanisms operative in photochemical molecular devices which combine a photosensitizer and a catalyst connected by an electron relay.[2–9] The operation of such molecular devices requires the presence of solvents, and as many molecular complexes are insoluble in aqueous media, often organic solvents are used.[5] Although it is known that the activity of photocatalysts is influenced by the properties of the solvent,[6] it is fair to say that a systematic understanding of this influence is still lacking. Here we show that the polarity of a solvent represented by its dielectric constant can strongly affect the electronic and thus also the photocatalytic properties of photoactive molecular complexes.

In particular ruthenium-based complexes such as $[(tbbpy)_2Ru(tpphz)PtI_2]^{2+}$ (tbbpy = 4,4′-di-*tert*-butyl-2,2′-bipyridine, tpphz = tetrapyrido[3,2-a:2′,3′-c:3‴‴-h:2‴,3‴-j]phenazine) denoted by $RuPtI_2$ in the following, have successfully been used as the photosensitizer in photochemical molecular devices.[4,5,10] $RuPtI_2$ is one of the most active supramolecular photocatalysts for hydrogen evolution incorporating photosensitizer, bridging ligand and catalysts within one molecular structure. The recently established novel active repair mechanism for this catalyst leads to a boost in attainable catalytic activity with triethylamine (TEA) as electron donor and acetonitrile water mixtures as solvents.[11] The catalytic efficiency of the light-driven hydrogen evolution reaction of $RuPtI_2$ and the related $RuPdCl_2$ is strongly dependent on several factors such as the nature of the sacrificial electron donor[12] and supramolecular

aggregation phenomena.[13–15] The interaction with polyaromatic supramolecular activators via $\pi - \pi$ bonding with the bridging ligand led to a reduction in the induction phase and an improved initial turnover frequency (TOF) and turnover number (TON) for $RuPdCl_2$.[13] The nature of the applied solvent mixtures has a profound effect on the attainable catalytic activity.[16–18] Whereas in pure acetonitrile-TEA mixtures TONs of 56 are possible, increasing the water content leads to TONs of more than 200. However, it is not clear whether these effects stem from manipulation of the photophysics of the light-driven electron transfer due to solvatochromic effects[16] or from substrate limitations for the actual catalytic hydrogen evolution process.[17,18]

Here we concentrate on solvatochromic effects caused by the medium surrounding the photocatalytically active complexes which may modify its electronic and optical properties. Rutheniumpolypyridyl complexes have been shown to exhibit a negative solvatochromism, i.e., a blueshift of the UV-vis absorption bands in water compared to organic solvents[19] which has been reproduced in time-dependent density functional theory calculations and has been related to a decreased dipole moment in the excited state.[20] Such a blue shift has also been obtained in TD-DFT calculations of ruthenium (II) polypyridine-type complexes.[21] Solvent-induced shifts are typically assumed to be due to dipole-dipole interactions between polar molecules and a polarizable medium,[22] as found for a wide range of molecules.[22–26]

We will show that also photocatalytic molecular devices such as $RuPtI_2$ can exhibit a strong solvatochromism. In this molecule, $[(tbbpy)_2Ru]^{2+}$ acts as the photosensitizer (PS), (tpphz) is the bridging ligand (BL) and PtI_2 the catalytically active center (CAT), as illustrated in Fig. 1. The expected photochemical mechanism in such photocatalysts is assumed to consist of the following steps: (i) A photon excites an electron in the Ru(II) metal center which creates a metal-to-ligand charge-transfer (MLCT) state residing at the bridging ligand and bipyridine, (ii) ultrafast intersystem crossing (ISC) and excited state relaxation processes generate a population of triplet MLCT state(s) localized on the tpphz bridging ligand, and (iii) an electron transfer to the PtI_2 catalyst occurs and forms a charge-separated

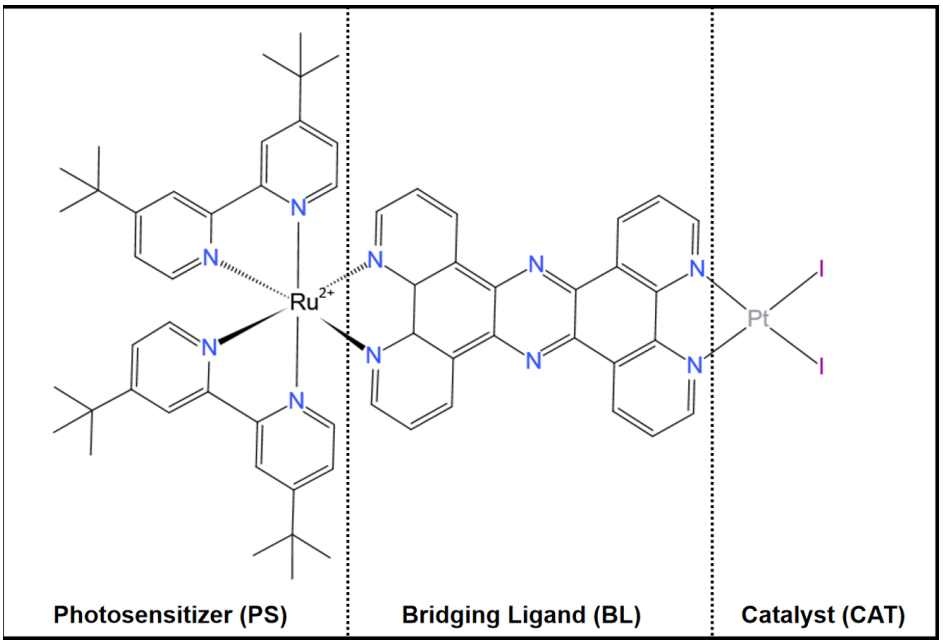

Figure 1: Illustration of the structure of the $RuPtI_2$ photocatalyst.

(CS) state.[27] As this photochemical molecular device consists of two metal centers, further complexity is added to the polarization mechanism responsible for solvatochromic effects. For example, electronic density can be shifted from the activated catalytic center to the bridging ligand upon visible-light irradiation thus reducing the catalytic activity.[28]

We will first present our quantum chemical calculations based on density functional theory (DFT) and time-dependent density functional theory (TDDFT) of the photocatalyst. The presence of the solvent has been taken into account using implicit solvent models. The findings of the quantum chemical calculations have been carefully analyzed in terms of the underlying electronic structure of the molecular complexes. Finally, we will discuss the implications of our findings for the operation of photochemical molecular devices.

2 Results and Discussion

As a first step, we determined the structure of the $RuPtI_2$ monomer complex in the gas phase and compared it with its optimized structure embedded in implicit solvents with dielectric constants up to ε = 78.36 corresponding to water. In detail, we have considered implicit

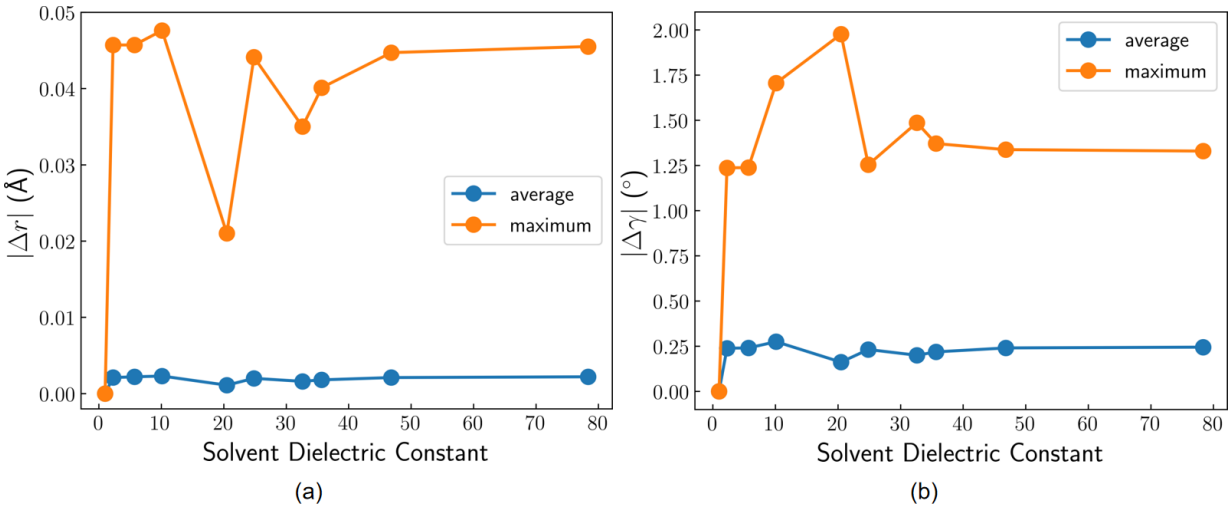

Figure 2: Maximum and average structural changes of the $RuPtI_2$ photocatalyst upon embedding it in various solvent compared to the optimum gas phase structure with respect to the bond distances (a) and the bond angles (b).

solvents with dielectric constants corresponding to benzene, chlorobenzene, dichloroethane (DCE), acetone, ethanol (EtOH), methanol (MeOH), acetonitrile (MeCN), dimethylsulphoxide (DMSO), and water. In order to quantify the structural changes due to the presence of the solvent, we determined the change in the bond lengths ($|\Delta r_i|$)

$$|\Delta r_i| = |r_i^{\text{solvent}} - r_i^{\text{gas}}|, \tag{1}$$

and the bond angles ($|\gamma_i|$)

$$|\Delta \gamma_i| = |\gamma_i^{\text{solvent}} - \gamma_i^{\text{gas}}|. \tag{2}$$

with respect to the various bond lengths and angles of the complex.

In Fig. 2, we plot both the maximum value and the mean value averaged over all bonds for the bond distances (panel a) and the bond angles (panel b) for all considered solutes. Overall we find rather small structural changes of the $RuPtI_2$ complex upon embedding it in the implicit solvent. On the average, the change in the bond angles is below 2.5×10^{-3} Å and the change in the bond angles is below 0.3°. Still, there are maximum changes of up to 0.05 Å in the bond distances and of up to 2° in the bond angles. Interestingly, these maximum changes

are found in the Pt-I distance and the I-Pt-I bond angle of the catalytically active PtI_2 moiety. Obviously, the presence of the implicit solvent has the largest impact on the rather ionic bonds of the catalysts protruding into the solvent. However, overall we can conclude that the presence of the solvent has only a small influence on the geometric structure of the photoactive complex.

In contrast to the structural properties, the electronic properties depend sensitively on the dielectric constant of the electrolyte. In Fig. 3a, the energy levels of the $RuPtI_2$ complex close to the HOMO-LUMO gap determined using the Gaussian 16 code[29] are plotted together with a color coding denoting the electron localization. First of all note that the HOMO levels are typically located at metal centers, whereas the LUMO levels belong to organic moieties. Very surprisingly, in the gas phase and for weakly polar electrolytes, the HOMO is localized at the catalyst and not at the Ru atom. Hence, in the gas-phase low-energy excitations do not originate from the photosensitizer, as usually expected, but rather from the catalyst. Only starting with dichloroethane, i.e. at $\varepsilon \approx 10$, the HOMO becomes localized at the metal center of the photoactive Ru-complex. In contrast, the LUMO is located at the phenazine part of the bridging ligand over the whole range of considered dielectric constants.

It is noteworthy that ruthenium complexes with oligopyridophenazine ligands show an optically accessible local LUMO at the ruthenium coordinated bipyridine part of the ligand and a LUMO which is significantly lower in energy at the phenazine moiety. Direct optical population of the latter is not feasible.[30] Upon photoactivation of the ruthenium center, the excited electron becomes transferred to the bridging ligand. However, in contrast to the typically assumed picture of the photochemical mechanism in photocatalysts,[27] at low dielectric constants the initial metal-to-ligand charge transfer does not occur from the Ru(II) metal center, but rather from the metal center of the catalyst. Figure 3a also reveals that all considered electronic levels move to higher energies with increasing dielectric constant. However, this dependence is least pronounced at the highest occupied state localized at the Pt center. As this state corresponds to the HOMO at low dielectric constants, this is the cause

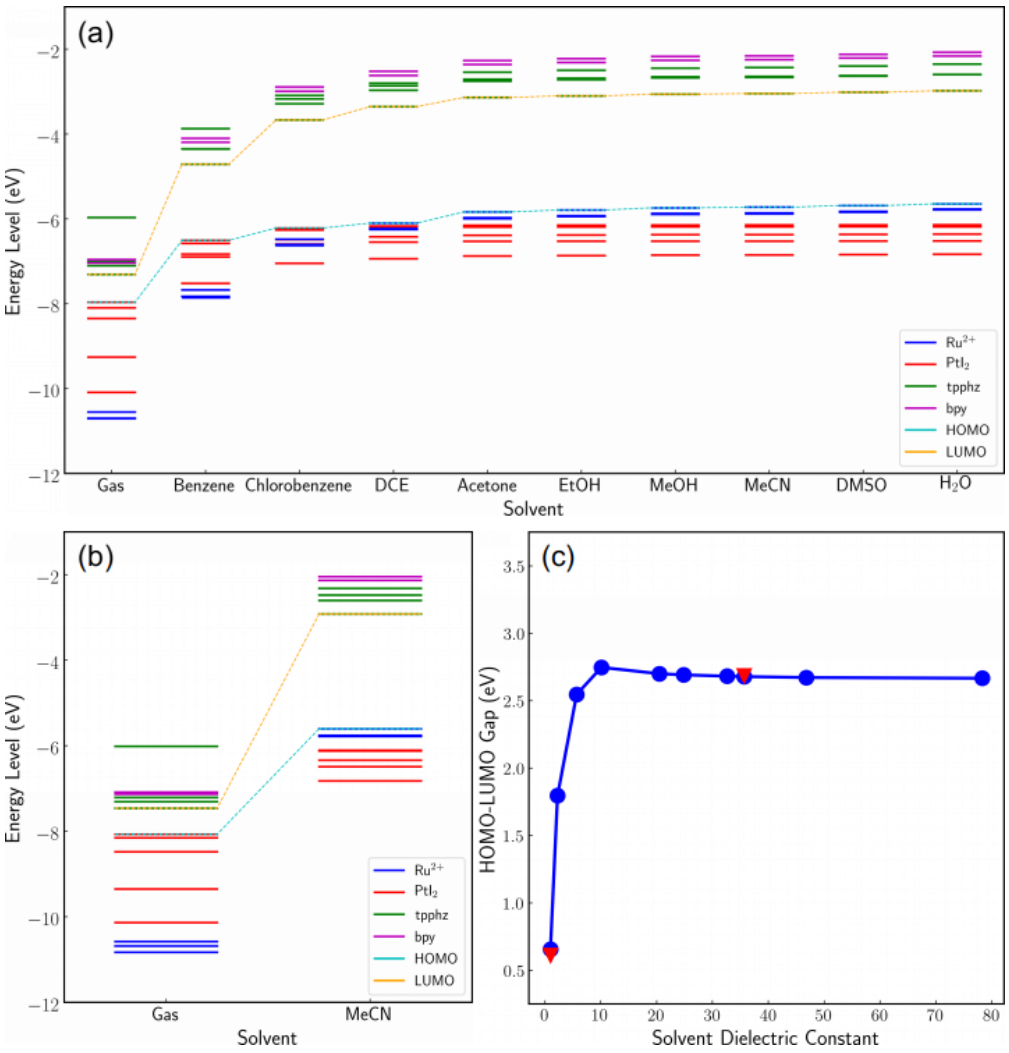

Figure 3: Calculated change of the electronic structure of the $RuPtI_2$ photocatalyst due to the presence of an implicit solvent. Occupied and unoccupied energy levels of the $RuPtI_2$ complex calculated using (a) the Gaussian 16 and (b) the FHI-AIMS code. The color coding indicates the projection of the one-particle states onto the Ru^{2+} metal center, the PtI_2 catalyst, the bridging ligand (tpphz) and bipyridine (bpy). The solvents are ordered according to their dielectric constant, and the corresponding HOMO and LUMO levels are connected by the yellow and light blue line, respectively. c) HOMO-LUMO gaps of $RuPtI_2$ as a function of the dielectric constant of the implicit solvent using both codes with the order of the solvents being the same as in panel a.

of the strong solvatochromism calculated in this system. Interestingly, such a variation of the HOMO-LUMO gap is also obtained when we consider the [(tpphz)PtI_2] complex formed by the bridging ligand and the PtI_2 catalyst alone. Hence the presence of the Ru(II) center apparently is not the main cause for the occurrence of the strong solvatochromic effect.

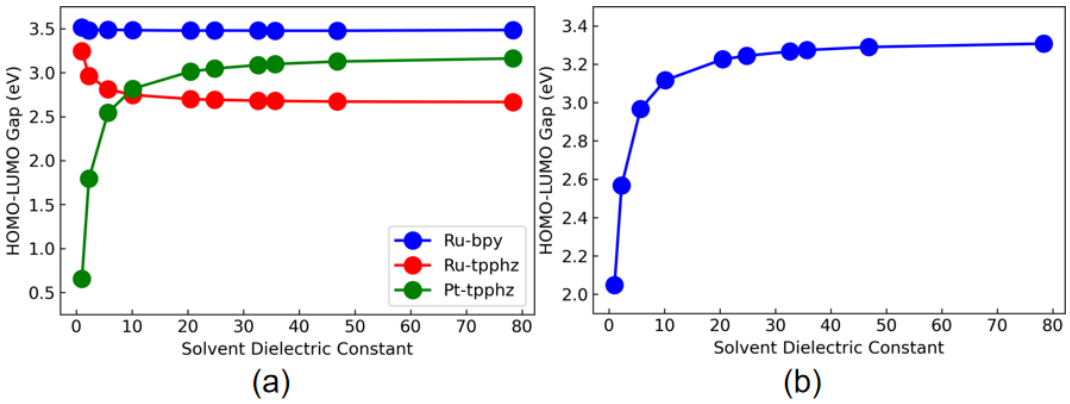

Figure 4: Local HOMO-LUMO gaps plotted as a function of the dielectric constant for (a) Ru-bpy, Ru-tpphz, and Pt-tpphz combinations and (b) for the Pt-tpphz pair of an isolated (tpphz)PtI_2 complex.

Figure 3b shows the same information as Fig. 3a, but obtained with the FHI-AIMS code[31] for the $RuPtI_2$ complex in gas phase and in acetonitrile (MeCN). The results are very similar to those obtained with the Gaussian 16 code, in particular as far as the levels close to the HOMO-LUMO gap are concerned. This illustrates the robustness of our computational findings with respect to the strong solvatochromic effects found for the $RuPtI_2$ complex. In Fig. 3c, finally the HOMO-LUMO gap is plotted as a function of the dielectric constant of the considered electrolytes. This panel illustrates that the HOMO-LUMO gap rises very strongly from 0.6 eV to 2.8 eV upon changing the dielectric constant from the gas-phase value of $\varepsilon \approx 1$ to $\varepsilon \approx 10$ corresponding to dichloroethane and then levels off at this value. This has to be related to the presence of the electric double layer forming at the interface between the photocatalytic complex and the electrolyte.[32]

In order to get some more insights into the nature of the solvatochromic effect, we have determined local HOMO-LUMO gaps for three different pairs, Ru-bpy, Ru-tpphz, and Pt-tpphz, which are plotted in Fig. 4a. The local Ru-bpy HOMO-LUMO gap located around the photosensitizer is almost independent of the dielectric constant in spite of the fact that the levels are shifted as a function of the dielectric constant. This is caused by the fact that HOMO and LUMO are shifted by almost the same amount, as also found for ruthenium polypyridine complexes[21] and other organometallic compounds.[33]

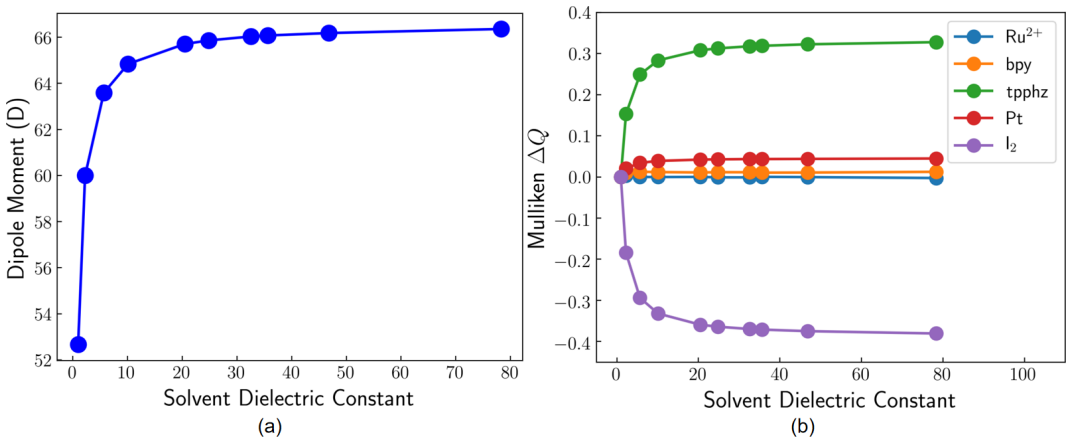

Figure 5: (a) Dipole moment and (b) Mulliken charge difference (ΔQ) of the $RuPtI_2$ complex as a function of dielectric constant of solvent.

In contrast, the local HOMO-LUMO gap decreases for the Ru-tpphz pair, whereas it increases for the Pt-tpphz pair for higher dielectric constants. A very similar increase is also observed for the Pt-tpphz pair of an isolated $[(tpphz)PtI_2]$ complex, i.e., with the photosensitizer removed from the complex (see Fig. 4b). Hence, apparently this increase is independent of the coupling to the photosensitizer. According to Fig. 4a, the minimum HOMO-LUMO gap changes at about $\varepsilon \sim 10$ from a Pt-tpphz to a Ru-tpphz transition, which means that in solvents with a low polarity the catalyst would possibly exhibit a higher photoactivity than the Ru complex.

As solvatochromism is usually assumed to be due to the dipole-dipole interactions between polar molecules and a polarizable medium,[22] it is instructive to take a closer look at the dipole moment and the charge redistribution within the $RuPtI_2$ complex upon changing the dielectric constant of the solvent. As Fig. 5a illustrates, there is a strong increase in the overall dipole moment of the whole complex from about 50 D to 66 D as a function of the polarity of the solvent. This increase strongly correlates with the opening up of the HOMO-LUMO gap shown in Fig. 3c as a function of dielectric constant. This suggests that the change in the dipole moment is directly related to the strong solvatochromism of the whole complex.

In order to understand the cause of the increasing dipole moment, we have performed

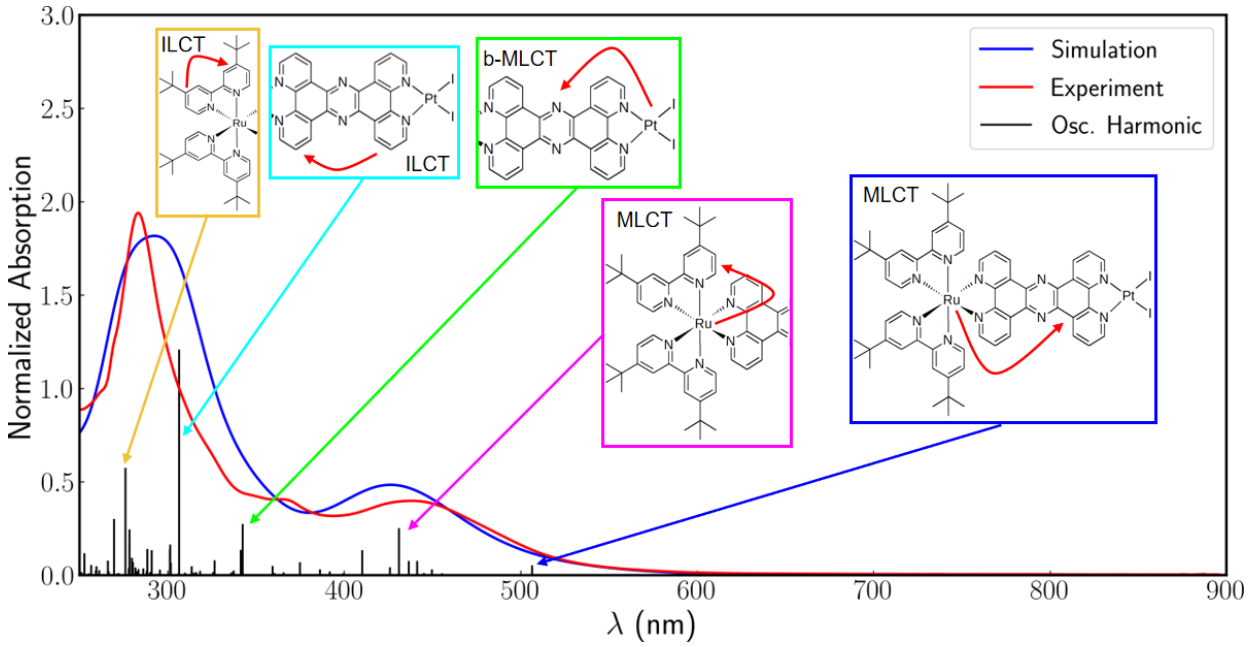

Figure 6: Experimental[4] and calculated absorption spectrum of $RuPtI_2$ in acetonitrile. The insets illustrate the overall charge transfer processes associated with five selected excitations derived from the calculations.

a Mulliken charge analysis focusing on five different parts of the photoactive complex, the Ru^{2+} ion, the bipyridine (bpy) moiety, the bridging ligand (tpphz), the Pt atom and the two iodine atoms. As Fig. 5b reveals, upon variation of the dielectric constant the Mullikan charges at the Ru^{2+} ion, bipyridine (bpy), and the Pt atom remain approximately constant. In contrast, there is a significant charge transfer from the two iodine atoms to the bridging ligand upon increasing the dielectric constant. These findings together with the analysis of the local HOMO-LUMO gap discussed above suggest that the strong solvatochromism found in the $RuPtI_2$ complex is mainly due to the properties of the PtI_2 catalyst together with the bridging ligand.

Still, as Fig. 3a reveals, the energy levels at the Ru^{2+} center, bipyridine, and tpphz strongly shift as a function of the dielectric constant. This might be an indication that the local charge at the Ru^{2+} and the ligands around Ru^{2+} are the cause for the overall shift of the energy levels whereas the local dipole moment between the bridging ligand and catalyst is responsible for the change of the HOMO-LUMO gap and thus the strong solvatochromism in this system.

In order to judge the quality of our calculations, we compare the absorption spectrum derived from the LR-TDDFT approach with the corresponding experimental results obtained in acetonitrile[4] in Fig. 6. The main calculated absorption peaks in the visible range at 437 nm and in the UV range at 300 nm compare well with the corresponding experimental results, 442 nm and 280 nm, respectively, giving credibility to our approach. In Fig. 6, we also identify the five main excitation mechanisms of the $RuPtI_2$ photocatalyst, namely the d(Ru) $\rightarrow \pi^*$(tpphz) (blue), d(Ru) $\rightarrow \pi^*$(bpy) (magenta), d(Pt), $n_I \rightarrow \pi^*$(tpphz) (green), π(tpphz) $\rightarrow \pi^*$(tpphz) (cyan), and π(bpy) $\rightarrow \pi^*$(bpy) (orange) transitions. Electronic isosurfaces of the frontier orbitals of the $RuPtI_2$ photocatalyst in the considered solvents indicating the localization of the orbitals are shown in Figs. S2-S11 in the supporting information. In the visible range, the peak at 437 nm represents the electronic excitation from the Ru ion to bipyridine, whereas the shoulder around 350-380 nm is related to the excitation from the catalyst to the bridging ligand. The UV peak at 300 nm is related to the superposition of intra-ligand charge transfer (ILCT) processes on the bridging ligand at 306 nm and in the bipyridine moiety at 277 nm.

Table 1: Properties of the main excitations of the solvated $RuPtI_2$ complexes in the considered solvents in the visible and UV region: wavelength in the visible (λ_{max}^{vis}) and in the UV region (λ_{max}^{UV}), excitation energy of the photosensitizer (E_{max}^{PS}) and from the catalyst to the bridging ligand (E_{max}^{ctbl}) together with their oscillator strengths f_{PS} and f_{ctbl}, respectively.

Solvent	ε	λ_{max}^{vis} (nm)	λ_{max}^{UV} (nm)	E_{max}^{PS} (eV)	f_{PS}	E_{max}^{ctbl} (eV)	f_{ctbl}
Gas Phase	1.00	427.00	328.00	2.73	0.16	2.01	0.14
			271.00				
Benzene	2.27	431.00	313.00	2.92	0.22	2.42	0.15
			278.00				
Chlorobenzene	5.70	436.00	289.00	2.91	0.13	2.85	0.20
Dichloroethane	10.12	434.00	285.00	2.87	0.18	3.02	0.12
Acetone	20.49	436.00	299.00	2.77	0.23	3.15	0.10
Ethanol	24.85	436.00	300.00	2.76	0.20	2.83	0.15
Methanol	32.61	436.00	300.00	2.76	0.18	3.20	0.14
Acetonitrile	35.69	435.00	300.00	2.77	0.18	3.21	0.13
DMSO	46.83	435.00	301.00	2.85	0.22	3.22	0.12
Water	78.36	435.00	301.00	2.85	0.20	3.25	0.12

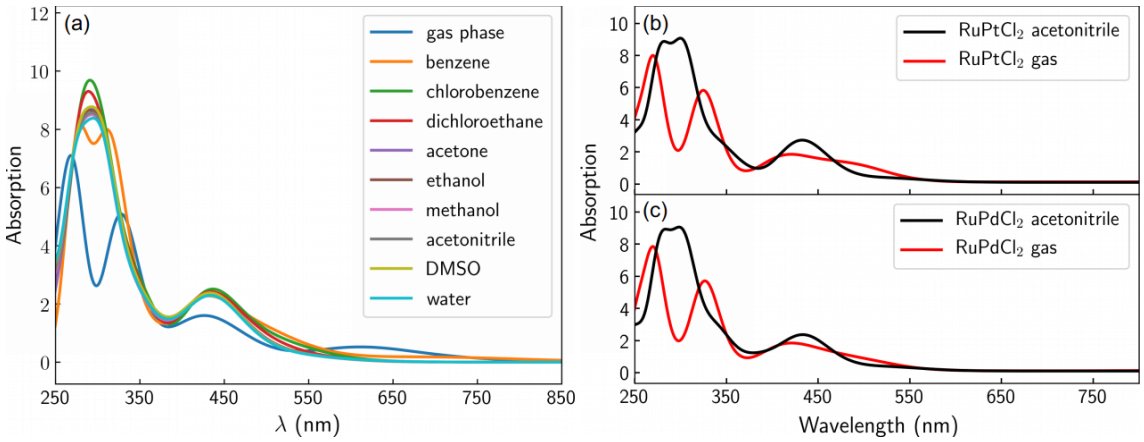

Figure 7: Calculated absorption spectra of (a) $RuPtI_2$ in various solvents, (b) $RuPtCl_2$ and (c) $RuPdCl_2$ in gas phase and acetonitrile.

The absorption spectra of the $RuPtI_2$ photocatalyst in various media within the UV-Vis range are shown in Fig. 7a, the single excitations are listed in the supporting information in Tab. S1-S10. Furthermore, we have collected the properties of the maximum excitations in the visible and the UV region in Tab. 1. Maximum absorption in the visible region occurs in the relatively narrow wavelength range between 428 and 438 nm (2.83-2.90 eV). The electronic excitation mechanisms are also basically the same, corresponding to d(Ru) $\rightarrow \pi^*$(tpphz) and d(Ru) $\rightarrow \pi^*$(bpy). Obviously, the solvent-solute interaction does not significantly influence the profile of the maximum excitation wavelengths of the $RuPtI_2$ photocatalysts within the visible light region.

In detail, in the visible region, by increasing the dielectric constant corresponding to the transition from gas phase to chlorobenzene, there is an increase of the wavelength λ_{max}^{vis} of the main absorption peak which then stays approximately constant at about 435 nm for larger dielectric constants. As listed in detail in the supporting information, these excitations mainly correspond to d(Ru) $\rightarrow \pi^*$(tpphz) and d(Ru) $\rightarrow \pi^*$(bpy) transitions, except for chlorobenzene, where the largest contribution comes from the d(Pt) $\rightarrow \pi^*$(tpphz).

In order to examine the effect of the solvent on the singlet excitations of the photosensitizer, we define the maximum excitation energy of the photosensitizer (E_{max}^{PS}) as the transition with the maximum oscillator strength f_{PS} restricted to the transitions d(Ru) $\rightarrow \pi^*$(tpphz)

and d(Ru) $\rightarrow \pi^*$(bpy) originating from the photosensitizer. According to Tab. 1, E_{max}^{PS} lies in the range 2.70–2.92 eV (453–424 nm). This means that the solvent variation does not significantly change the excitation energy of the photosensitizer, as the maximum singlet absorption in the photosensitizer stays in the wavelength range of blue light for all considered dielectric constants. Interestingly enough, for low dielectric constants corresponding to gas phase and benzene, in the UV region two ILCT peaks corresponding to the π(tpphz) $\rightarrow$ π^*(tpphz) and π(bpy) $\rightarrow \pi^*$(bpy) transition are observed which merge to one peak at higher dielectric constants.

According to Fig. 7a, in gas phase and benzene the peaks at about 270 nm associated with the $\pi - \pi^*$ excitation on the bipyridine moiety have a higher intensity than the corresponding excitation on tpphz at about 320 nm. As just mentioned, for higher dielectric constants of the solvent, only one peak appears in this region. This phenomenon is caused by the slight shift of the $\pi - \pi^*$ transition on tetrapyrido phenazine from 3.9 eV to about 4.0 eV. On the other hand, the π(bpy) $\rightarrow \pi^*$(bpy) transition tends to stay constant at $\sim$4.4 eV. Thus these two ILCT states shift closer together resulting in only one overall peak. Furthermore, based on our TDDFT calculations we speculate that the small blue shift of the π(tpphz) $\rightarrow \pi^*$(tpphz) transition is probably related to the higher charge transfer to the bridging ligand for more polar solvents.

A rather similar qualitative behavior was observed in experiments in which gas-phase UV/Vis photofragmentation spectra where compared with normalized absorption spectra in acetonitrile solution, however, for $RuPdCl_2$ and $RuPtCl_2$ photocatalysts.[34] In order to check whether the results for $RuPdCl_2$ and $RuPtCl_2$ photocatalysts are also relevant for the understanding of the $RuPtI_2$ system we are focusing on here, we additionally performed LR-TDDFT calculations to determine the absorption spectra of the $RuPtCl_2$ and $RuPdCl_2$ complexes in gas phase and acetonitrile, see Fig. 7b and c. Similar to the results for the $RuPtI_2$ system, we observe two peaks in the gas phase and only one in acetonitrile for both photocatalysts. And again, the peaks in the UV region mainly originate from ILCTs in

tetrapyrido phenazine and bipyridine. In addition, a MLCT peak is observed at ~ 440 nm, whereas a backward MLCT (b-MLCT) process from the catalyst to tetrapyrido phenazine (d(Pt), $n_I \rightarrow \pi^*$(tpphz)) leads to a shoulder at around 350 nm, in agreement with the experiment.[4,34,35] This nice agreement with the experiment for the $RuPdCl_2$ and $RuPtCl_2$ complexes suggests that our calculations for the $RuPtI_2$ complex are trustworthy, exhibiting a predictive power.

We now take a closer look at the backward MLCT (b-MLCT) from the catalyst to tetrapyrido phenazine (d(Pt), $n_I \rightarrow \pi^*$(tpphz)). As documented in the supporting information, a b-MLCT exists in solvents with small dielectric constants in the near-IR region up to the visible region, indicating a photopoisoning effect. In solvents with high dielectric constants, on the other hand, b-MLCT occurs at wavelengths around 350 nm and shows up in measured spectra as a shoulder at this wavelength.[4] To quantify the behaviour of the b-MLCT, we define E_{max}^{ctbl} as the energy of the b-MLCT with maximum oscillator strength which are listed Tab. 1. We find that E_{max}^{ctbl} exhibits a blue-shift from 615 to 381 nm (2.01 to 3.25 eV) upon increasing the dielectric constant of the solvent from 1 to 80.

The b-MLCT from the catalyst metal center (Pt) to the bridging ligand is of importance as the efficiency of photocatalytic processes might also be influenced by such processes.[28] Electron transfer from the catalytic center to the bridging ligand can reduce the catalytic activity.[28] Hence, the b-MLCT transition should be energetically more demanding than the MLCT transition in order to suppress it. Indeed, as Tab. 1 shows, increasing the dielectric constant of the solvent to values above 10 shifts the excitation energy of the b-MLCT to the higher energy than those associated with the MLCT.

Besides addressing singlet transitions in the $RuPtI_2$ complex in various solvents, we have also considered singlet-triplet transitions which can play an important role in the excited state relaxation processes populating triplet MLCT states upon ultra-fast intersystem crossing.[27,28,36–38] The properties of the most dominant triplet excitations for the various solvents considered in this work are collected in the supporting information in Tabs. S6-S24. In gen-

eral, we find trends in the excitations that are qualitatively rather similar to the singlet transitions, therefore we do no discuss them here in detail.

Overall, we find dramatic differences in the electronic properties of the $RuPtI_2$ complex embedded in an implicit solvent with low and high dielectric constants constants. The HOMO-LUMO gap, the dipole moment and the charge of the $RuPtI_2$ complex in the singlet state change rather significantly at low dielectric constants upon increasing the dielectric constant (see Figs. 3-5). In total, all these changes appear to be a consequence of the charge rearrangement between the tpphz bridging ligand and the two iodine atoms of the catalytically active center upon embedding the $RuPtI_2$ complex in a polarizable medium (see Fig. 5b). As these solvatochromic effects can be used to tailor the electronic properties of photoactive complexes, it appears to be worthwhile to also look for such a solvatochromism in other photoactive and photocatalytic complexes.

3 Conclusions

Based on density functional theory (DFT) and time-dependent DFT calculations, we have studied the properties of a $RuPtI_2$ molecular photocatalyst upon embedding it in an implicit solvent as a function of its dielectric constant. Whereas the geometric structure of the $RuPtI_2$ complex is hardly influenced by this embedding, the electronic properties change dramatically upon increasing the dielectric constant from 1 to 20 corresponding to the transition from gas phase conditions to solvation in acetone. For higher dielectric constants, the properties then remain approximately constant. These dramatic changes at low dielectric constants are associated with a change of the location of the HOMO state from the PtI_2 catalyst to the photoactive Ru center and a strong increase of the HOMO-LUMO gap. Based on an analysis of the charge and spin distribution, we relate these changes to the net electron transfer from the bridging ligand to the iodine atoms upon embedding the $RuPtI_2$ complex in a polarizable medium. As a consequence, we predict strong solvatochromism in this

complex. Such dramatic effects might well also occur in other photoactive and photocatalytic complexes upon solvation. As the integration of photocatalysts in very unpolar polymeric materials, lipid membranes etc. is an area of increasing relevance, integration of $RuPtI_2$ and similar photocatalysts in such materials has to be treated with caution as a complete switch of the light-induced electron transfer mechanisms might occur. However, in general our results suggest that such strong solvatochromic effects might be used to deliberately tailor the properties of photoactive complexes.

4 Computational details

In order to unravel the effect of the interaction between molecular $RuPtI_2$ photocatalysts and its surrounding medium, we have performed DFT and TDDFT calculations using the Gaussian 16 code.[29] The electronic ground-state properties of the $RuPtI_2$ complexes in the singlet and triplet configurations were determined using DFT calculations employing the B3LYP functional[39,40] to account for the exchange-correlation effects using the def2svp basis set[41,42] for all atoms. To take dispersion interaction into account, the D3 dispersion scheme of Grimme with Becke-Johnson damping was used in this work.[43,44] Some additional calculations have also been performed with the FHI-AIMS code.[31] In the AIMS calculations, the tight basis set was employed for the B3LYP geometry optimization and energy level calculations. Relativistic effects have been considered on the level of the atomic zeroth order regular approximation (ZORA).[45] Furthermore, the van der Waals correction scheme by Tkatchenko and Scheffler (vdW-TS) was used.[46] To model the presence of the electrolyte in the AIMS calculation, we used the multipole moment expansion (MPE) implicit solvation method.[47] Using test sets from Marenich et. al.,[48] we selected the solvation parameters α = 2.89 meV/Å^2, β = −3.12 meV/Å^3 and the cavity isodensity ρ_{iso} = 40.00 meV/Å^3[49] for acetonitrile. Further details of this procedure are given in the supporting information.

In the Gaussian calculations, the SMD (Solvation Model Based on Density) continuum

solvation model[48] was applied to describe the solvent around the complex as it gives more reliable values of the solvation free energies (ΔG_{sol}) of cationic complexes compared to other methods such as the integral-equation-formalism polarizable continuum model (IEFPCM) or conductor-like polarizable continuum models (CPCM).[48] Furthermore, it also promises a more realistic representation of the molecule-solvent interaction as also other properties such as Abraham's hydrogen bond acidity and basicity, aromaticity, and electronegative halogenicity have entered its construction.[29,48] The particular solvents addressed in this work are characterized by their respective dielectric constant. In detail, we considered benzene (ε = 2.27), chlorobenzene (ε = 5.70), dichloroethane (DCE, ε = 10.12), acetone (ε = 20.49), ethanol (EtOH, ε = 24.85), methanol (MeOH, ε = 32.61), acetonitrile (MeCN, ε = 35.69), dimethylsulphoxide (DMSO, ε = 46.83) and water (ε = 78.36). Furthermore, the corresponding results are also compared with gas phase calculations (gas, ε = 1.00) calculations.

The optical properties of the $RuPtI_2$ complexes were derived using a linear response formalism based on Time Dependent Density Functional Theory (LR-TDDFT)[50,51] within the singlet ground-state geometry of the complexes. The absorption spectra of the $RuPtI_2$ complexes were determined using

$$\varepsilon(E) = \sum_{i}^{n} \frac{f}{\sigma} \exp\left(- \frac{E - E_i}{\sigma} \right)^2 , \tag{3}$$

where $\varepsilon(E)$ corresponds to the absorption spectra at energy E, f is the oscillator harmonic strength derived in the TDDFT calculations, and σ denotes the broadening of the absorption spectra.[29] In this work, we selected σ = 0.30 eV in order to mimic the typical resolution of experiments.

5 Acknowledgments

We thank the German Research Foundation (DFG) for financial support through Project C5 of the Transregional Collaborative Research Centre TRR234 CataLight (Project No.

364549901). B.B. acknowledges support by the Studienstiftung des Deutschen Volkes for a PhD scholarship. Computer time provided by the state of Baden-Württemberg through the bwHPC project and by the DFG under grant no INST 40/575-1 FUGG (JUSTUS 2 cluster) is gratefully acknowledged. This work contributes to the research performed at CELEST (Center for Electrochemical Energy Storage Ulm-Karlsruhe).

References

(1) Schlögl, R. The Role of Chemistry in the Energy Challenge. *ChemSusChem* **2010**, *3*, 209–222.

(2) Balzani, V.; Juris, A.; Venturi, M.; Campagna, S.; Serroni, S. Luminescent and Redox-Active Polynuclear Transition Metal Complexes. *Chem. Rev.* **1996**, *96*, 759–834.

(3) Andreiadis, E. S.; Chavarot-Kerlidou, M.; Fontecave, M.; Artero, V. Artificial Photosynthesis: From Molecular Catalysts for Light-driven Water Splitting to Photoelectrochemical Cells. *Photochem. Photobiol.* **2011**, *87*, 946–964.

(4) Pfeffer, M. G.; Kowacs, T.; Wächtler, M.; Guthmuller, J.; Dietzek, B.; Vos, J. G.; Rau, S. Optimization of Hydrogen-Evolving Photochemical Molecular Devices. *Angew. Chem. Int. Ed.* **2015**, *54*, 6627–6631.

(5) Kaufhold, S.; Petermann, L.; Staehle, R.; Rau, S. Transition metal complexes with N-heterocyclic carbene ligands: From organometallic hydrogenation reactions toward water splitting. *Coord. Chem. Rev.* **2015**, *304-305*, 73–87.

(6) Dalle, K. E.; Warnan, J.; Leung, J. J.; Reuillard, B.; Karmel, I. S.; Reisner, E. Electro- and Solar-Driven Fuel Synthesis with First Row Transition Metal Complexes. *Chem. Rev.* **2019**, *119*, 2752–2875.

(7) Sen, A.; Kupfer, S.; Gräfe, S.; Groß, A. The role of anchoring groups in ruthenium(II)-bipyridine sensitized p-type semiconductor solar cells—a quantum chemical approach. *J. Phys. B: At. Mol. Opt. Phys.* **2020**, *53*, 234001.

(8) Wahyuono, R. A.; Seidler, B.; Bold, S.; Dellith, A.; Dellith, J.; Ahner, J.; Wintergerst, P.; Lowe, G.; Hager, M. D.; Wächtler, M.; Streb, C.; Schubert, U. S.; Rau, S.; Dietzek, B. Photocathodes beyond NiO: charge transfer dynamics in a π-conjugated polymer functionalized with Ru photosensitizers. *Sci. Rep.* **2021**, *11*, 2787.

(9) Putra, M. H.; Seidenath, S.; Kupfer, S.; Gräfe, S.; Groß, A. Coupling of photoactive transition metal complexes to a functional polymer matrix. *Chem. Eur. J.* **2021**, *27*, 17104–17114.

(10) Sen, A.; Groß, A. Promising sensitizers for dye sensitized solar cells: A comparison of Ru(II) with other earth's scarce and abundant metal polypyridine complexes. *Int. J. Quant. Chem.* **2019**, *119*, e25963.

(11) Pfeffer, M. G. et al. Active repair of a dinuclear photocatalyst for visible-light-driven hydrogen production. *Nat. Chem.* **2022**, *14*, 500–506.

(12) Habermehl, J.; Nauroozi, D.; Martynow, M.; Vilk, Y. E.; Beranek, R.; Guthmuller, J.; Rau, S. Synthesis and hydrogen evolving catalysis of a panchromatic photochemical molecular device. *Sustainable Energy Fuels* **2020**, *4*, 619–624.

(13) Pfeffer, M. G.; Pehlken, C.; Staehle, R.; Sorsche, D.; Streb, C.; Rau, S. Supramolecular activation of a molecular photocatalyst. *Dalton Trans.* **2014**, *43*, 13307–13315.

(14) Mengele, A. K.; Weixler, D.; Chettri, A.; Maurer, M.; Huber, F. L.; Seibold, G. M.; Dietzek, B.; Eikmanns, B. J.; Rau, S. Switching the Mechanism of NADH Photooxidation by Supramolecular Interactions. *Chem. Eur. J.* **2021**, *27*, 16840–16845.

(15) Pehlken, C.; Pfeffer, M. G.; Reich, K.; Rau, S. Evaluation of 1H-NMR Spectroscopy-Based Quantification Methods of the Supramolecular Aggregation of a Molecular Photosensitizer. *Photochem. Photobiol.* **2022**, *98*, 1255–1263.

(16) Rau, S.; Schäfer, B.; Gleich, D.; Anders, E.; Rudolph, M.; Friedrich, M.; Görls, H.; Henry, W.; Vos, J. G. A Supramolecular Photocatalyst for the Production of Hydrogen and the Selective Hydrogenation of Tolane. *Angew. Chem. Int. Ed.* **2006**, *45*, 6215–6218.

(17) Herrmann, C.; Neugebauer, J.; Presselt, M.; Uhlemann, U.; Schmitt, M.; Rau, S.; Popp, J.; Reiher, M. The First Photoexcitation Step of Ruthenium-Based Models for Artificial Photosynthesis Highlighted by Resonance Raman Spectroscopy. *J. Phys. Chem. B* **2007**, *111*, 6078–6087.

(18) Tschierlei, S.; Karnahl, M.; Presselt, M.; Dietzek, B.; Guthmuller, J.; González, L.; Schmitt, M.; Rau, S.; Popp, J. Photochemical Fate: The First Step Determines Efficiency of H2 Formation with a Supramolecular Photocatalyst. *Angew. Chem. Int. Ed.* **2010**, *49*, 3981–3984.

(19) Nazeeruddin, M. K.; Zakeeruddin, S. M.; Humphry-Baker, R.; Jirousek, M.; Liska, P.; Vlachopoulos, N.; Shklover, V.; Fischer, C.-H.; Grätzel, M. Acid-Base Equilibria of (2,2'-Bipyridyl-4,4'-dicarboxylic acid)ruthenium(II) Complexes and the Effect of Protonation on Charge-Transfer Sensitization of Nanocrystalline Titania. *Inorg. Chem.* **1999**, *38*, 6298–6305.

(20) Fantacci, S.; De Angelis, F.; Selloni, A. Absorption Spectrum and Solvatochromism of the [Ru(4,4'-COOH-2,2'-bpy)2(NCS)2] Molecular Dye by Time Dependent Density Functional Theory. *J. Am. Chem. Soc.* **2003**, *125*, 4381–4387.

(21) Charlot, M.-F.; Aukauloo, A. Highlighting the Role of the Medium in DFT Analysis of

the Photophysical Properties of Ruthenium(II) Polypyridine-Type Complexes. *J. Phys. Chem. A* **2007**, *111*, 11661–11672.

(22) Reichardt, C. Solvatochromic Dyes as Solvent Polarity Indicators. *Chem. Rev.* **1994**, *94*, 2319–2358.

(23) Marini, A.; Muñoz Losa, A.; Biancardi, A.; Mennucci, B. What is Solvatochromism? *J. Phys. Chem. B* **2010**, *114*, 17128–17135.

(24) Masternak, A.; Wenska, G.; Milecki, J.; Skalski, B.; Franzen, S. Solvatochromism of a Novel Betaine Dye Derived from Purine. *J. Phys. Chem. A* **2005**, *109*, 759–766.

(25) Liu, T.; Han, W.-G.; Himo, F.; Ullmann, G. M.; Bashford, D.; Toutchkine, A.; Hahn, K. M.; Noodleman, L. Density Functional Vertical Self-Consistent Reaction Field Theory for Solvatochromism Studies of Solvent-Sensitive Dyes. *J. Phys. Chem. A* **2004**, *108*, 3545–3555.

(26) Krawczyk, P. Time-dependent density functional theory calculations of the solvatochromism of some azo sulfonamide fluorochromes. *J. Mol. Model.* **2015**, *21*, 118.

(27) Martynow, M.; Kupfer, S.; Rau, S.; Guthmuller, J. Excited state properties of a series of molecular photocatalysts investigated by time dependent density functional theory. *Phys. Chem. Chem. Phys.* **2019**, *21*, 9052–9060.

(28) Zedler, L.; Mengele, A. K.; Ziems, K. M.; Zhang, Y.; Wächtler, M.; Gräfe, S.; Pascher, T.; Rau, S.; Kupfer, S.; Dietzek, B. Unraveling the Light-Activated Reaction Mechanism in a Catalytically Competent Key Intermediate of a Multifunctional Molecular Catalyst for Artificial Photosynthesis. *Angew. Chem. Int. Ed.* **2019**, *58*, 13140–13148.

(29) Frisch, M. J. et al. Gaussian 16 Revision C.01. 2016; Gaussian Inc. Wallingford CT.

(30) Brennaman, M. K.; Alstrum-Acevedo, J. H.; Fleming, C. N.; Jang, P.; Meyer, T. J.; Papanikolas, J. M. Turning the $[Ru(bpy)_2dppz]^{2+}$ Light-Switch On and Off with Temperature. *J. Am. Chem. Soc.* **2002**, *124*, 15094–15098.

(31) Blum, V.; Gehrke, R.; Hanke, F.; Havu, P.; Havu, V.; Ren, X.; Reuter, K.; Scheffler, M. Ab initio molecular simulations with numeric atom-centered orbitals. *Comp. Phys. Comm.* **2009**, *180*, 2175–2196.

(32) Groß, A.; Sakong, S. Modelling the electric double layer at electrode/electrolyte interfaces. *Curr. Opin. Electrochem.* **2019**, *14*, 1–6.

(33) Miresmaeili, S. A.; Ghiasi, R. Theoretical study of solvent effect on the ligand field parameter in [M(CO)6]n complexes (M = V–, Cr, Mn+, Fe2+). *Russ. J. Phys. Chem.* **2017**, *91*, 1026–1036.

(34) Imanbaew, D.; Lang, J.; Gelin, M. F.; Kaufhold, S.; Pfeffer, M. G.; Rau, S.; Riehn, C. Pump-Probe Fragmentation Action Spectroscopy: A Powerful Tool to Unravel Light-Induced Processes in Molecular Photocatalysts. *Angew. Chem. Int. Ed.* **2017**, *56*, 5471–5474.

(35) Pfeffer, M. G.; Schäfer, B.; Smolentsev, G.; Uhlig, J.; Nazarenko, E.; Guthmuller, J.; Kuhnt, C.; Wächtler, M.; Dietzek, B.; Sundström, V.; Rau, S. Palladium versus Platinum: The Metal in the Catalytic Center of a Molecular Photocatalyst Determines the Mechanism of the Hydrogen Production with Visible Light. *Angew. Chem. Int. Ed.* **2015**, *54*, 5044–5048.

(36) Mengele, A. K.; Müller, C.; Nauroozi, D.; Kupfer, S.; Dietzek, B.; Rau, S. Molecular Scylla and Charybdis: Maneuvering between pH Sensitivity and Excited-State Localization in Ruthenium Bi(benz)imidazole Complexes. *Inorg. Chem.* **2020**, *59*, 12097–12110.

(37) Giannoudis, E.; Bold, S.; Müller, C.; Schwab, A.; Bruhnke, J.; Queyriaux, N.; Gablin, C.; Leonard, D.; Saint-Pierre, C.; Gasparutto, D.; Aldakov, D.; Kupfer, S.;

Artero, V.; Dietzek, B.; Chavarot-Kerlidou, M. Hydrogen Production at a NiO Photocathode Based on a Ruthenium Dye-Cobalt Diimine Dioxime Catalyst Assembly: Insights from Advanced Spectroscopy and Post-operando Characterization. *ACS Appl. Mater. Interfaces* **2021**, *13*, 49802–49815.

(38) Nair, S. S.; Bysewski, O. A.; Kupfer, S.; Wächtler, M.; Winter, A.; Schubert, U. S.; Dietzek, B. Excitation Energy-Dependent Branching Dynamics Determines Photostability of Iron(II) Mesoionic Carbene Complexes. *Inorg. Chem.* **2021**, *60*, 9157–9173.

(39) Lee, C.; Yang, W.; Parr, R. G. Development of the Colle-Salvetti correlation-energy formula into a functional of the electron density. *Phys. Rev. B* **1988**, *37*, 785–789.

(40) Becke, A. D. Density functional thermochemistry. III. The role of exact exchange. *J. Chem. Phys.* **1993**, *98*, 5648–5652.

(41) Weigend, F.; Ahlrichs, R. Balanced basis sets of split valence, triple zeta valence and quadruple zeta valence quality for H to Rn: Design and assessment of accuracy. *Phys. Chem. Chem. Phys.* **2005**, *7*, 3297–3305.

(42) Weigend, F. Accurate Coulomb-fitting basis sets for H to Rn. *Phys. Chem. Chem. Phys.* **2006**, *8*, 1057–1065.

(43) Grimme, S.; Ehrlich, S.; Goerigk, L. Effect of the damping function in dispersion corrected density functional theory. *J. Comp. Chem.* **2011**, *32*, 1456–1465.

(44) Mahlberg, D.; Sakong, S.; Forster-Tonigold, K.; Groß, A. Improved DFT Adsorption Energies with Semiempirical Dispersion Corrections. *J. Chem. Theory Comput.* **2019**, *15*, 3250–3259.

(45) van Lenthe, E.; Baerends, E. J.; Snijders, J. G. Relativistic total energy using regular approximations. *J. Chem. Phys.* **1994**, *101*, 9783–9792.

(46) Tkatchenko, A.; Scheffler, M. Accurate Molecular Van Der Waals Interactions from Ground-State Electron Density and Free-Atom Reference Data. *Phys. Rev. Lett.* **2009**, *102*, 073005.

(47) Sinstein, M.; Scheurer, C.; Matera, S.; Blum, V.; Reuter, K.; Oberhofer, H. Efficient Implicit Solvation Method for Full Potential DFT. *J. Chem. Theory Comput.* **2017**, *13*, 5582–5603, PMID: 28910530.

(48) Marenich, A. V.; Cramer, C. J.; Truhlar, D. G. Universal Solvation Model Based on Solute Electron Density and on a Continuum Model of the Solvent Defined by the Bulk Dielectric Constant and Atomic Surface Tensions. *J. Phys. Chem. B* **2009**, *113*, 6378–6396, PMID: 19366259.

(49) Hille, C.; Ringe, S.; Deimel, M.; Kunkel, C.; Acree, W. E.; Reuter, K.; Oberhofer, H. Generalized molecular solvation in non-aqueous solutions by a single parameter implicit solvation scheme. *J. Chem. Phys.* **2019**, *150*, 041710.

(50) Adamo, C.; Jacquemin, D. The calculations of excited-state properties with Time-Dependent Density Functional Theory. *Chem. Soc. Rev.* **2013**, *42*, 845–856.

(51) Laurent, A. D.; Adamo, C.; Jacquemin, D. Dye chemistry with time-dependent density functional theory. *Phys. Chem. Chem. Phys.* **2014**, *16*, 14334–14356.